Impact of W doping on Fe-rich (Mn,Fe)$_2$(P,Si) based giant magnetocaloric materials

Zhang, Fengqi; Smits, Sebastian; Kiecana, Anika; Batashev, Ivan; Shen, Qi; van Dijk, Niels; Brück, Ekkes

Citation (APA)
Zhang, F., Smits, S., Kiecana, A., Batashev, I., Shen, Q., van Dijk, N., & Brück, E. (2023). Impact of W doping on Fe-rich (Mn,Fe)$_2$(P,Si) based giant magnetocaloric materials. *Journal of Alloys and Compounds*, *933*, Article 167802. https://doi.org/10.1016/j.jallcom.2022.167802

Important note
To cite this publication, please use the final published version (if applicable).
Please check the document version above.

Impact of W doping on Fe-rich (Mn,Fe)₂(P,Si) based giant magnetocaloric materials

Fengqi Zhang *, Sebastian Smits, Anika Kiecana, Ivan Batashev, Qi Shen, Niels van Dijk, Ekkes Brück

Fundamental Aspects of Materials and Energy (FAME), Faculty of Applied Sciences, Delft University of Technology, Delft, the Netherlands

A B S T R A C T

The influence of doping with the $5d$ transition metal W has been studied in the quaternary $(Mn,Fe)_2(P,Si)$ based giant magnetocaloric compounds, which is one of the most promising systems for magnetic refrigeration. It is found that W substitution can separately decrease the Curie temperature T_C and retain the thermal hysteresis ΔT_{hys} at an almost constant level (∼5 K) for $Mn_{0.6}Fe_{1.27-x}W_xP_{0.64}Si_{0.36}$ ($x \leq 0.02$). Low-content W doping conserves the good magnetocaloric effect (MCE) without an obvious degradation. For $x \leq 0.02$ the average magnetic entropy change $|\Delta S_m|$ amounts to 11.4 Jkg⁻¹K⁻¹ for an applied magnetic field change of 2 T and the adiabatic temperature change ΔT_{ad} amounts to 3.9 K for an applied magnetic field change of 1.5 T. The occupancy of substitutional W atoms is determined by XRD experiments and DFT calculations. Our studies provide a good strategy to further optimize the MCE of this material family.

1. Introduction

The hexagonal Fe₂P-tpye (Mn,Fe)₂(P,Si) based magnetocaloric materials (MCMs) demonstrate an excellent giant magnetocaloric effect (GMCE) under low applied magnetic fields (e.g. 2 T) as a result of the strong magnetoelastic coupling [1,2]. Different promising application scenarios such as magnetic refrigeration [3], magnetic heat pumps [4,5] and thermomagnetic generators [6,7] have been proposed based on this material system because it is rare-earth free, contains no toxic elements, is commercially cheap and has a tunable T_C.

Different optimization strategies have been applied to further control the GMCE performance of (Mn,Fe)₂(P,Si) based MCMs, such as tuning the metal-metal or nonmetal-nonmetal ratios [8,9], chemical pressure engineering (substitutional/interstitial doping) including doping with light elements (Li, B, C, N, F, S) [10–12], $3d$ transition metal elements (V, Co, Ni, Cu, Zn) [13–15], $4d$ transition metal elements (Zr, Nb, Mo, Ru) [16–19] and other elements (Al, Ge, As) [1,20–22], and nano-structuring [23]. However, the alloying with doping elements simultaneously tunes T_C (towards higher T_C for Li, B, C, Al, Ge, Zn and Zr; towards lower T_C for N, F, S, V, Ni, Co, Cu, Ge, Nb, Mo and Ru) and changes ΔT_{hys} (which is detrimental to the cooling/heating efficiency) [24]. In several cases, like B, V, Nb and

Mo, doping can result in a shift from the first-order magnetic transition (FOMT) with a finite ΔT_{hys} to the critical point between the FOMT and second-order magnetic transition (SOMT) with a negligible ΔT_{hys}, while F doping makes the FOMT stronger with a larger ΔT_{hys}. The aim for the design of the MCMs is to simultaneously tune T_C, control ΔT_{hys} to a low value and maintain the GMCE performance. Considering the design of active magnetic regenerator (AMR) beds based on MCMs [25], once the optimal candidate compound (pure Mn-Fe-P-Si quaternary alloy) is identified it is crucial to find a simple strategy to regulate T_C and maintain the GMCE property without degradation.

Here we report that the $5d$ transition element W has successfully been introduced into Fe-rich $Mn_{0.6}Fe_{1.27-x}W_xP_{0.64}Si_{0.36}$ (x = 0.00, 0.01, 0.02, 0.03, 0.04, 0.05) materials. The thermodynamic, magnetic, crystallographic and microstructural properties have been investigated. It is found that a low content of W doping ($x \leq 0.02$) can decrease T_C, while keeping ΔT_{hys} constant and conserving the GMCE properties. However, for higher W contents ($x \geq 0.03$) the GMCE is continuously weakened due to the formation of an Fe₃W₃C based impurity phase, as observed in X-Ray Diffraction (XRD) and Scanning Electron Microscopy (SEM). Combined XRD experiments and Density Functional Theory (DFT) calculations identified that the W atoms are introduced in the main phase as substitutional element on the 3 g (Fe) site. The underlying mechanism is discussed in terms of the competition between the exchange interaction and covalent bonding. Our present study makes it possible to further optimize the magnetoelastic coupling in (Mn,Fe)₂(P,Si) based MCMs by W

* Corresponding author.
  E-mail address: F.Zhang-7@tudelft.nl (F. Zhang).

substitution, which reinforces its potential for magnetic cooling/heating applications.

2. Experimental procedure

The off-stoichiometric bulk $Mn_{0.6}Fe_{1.27-x}W_xP_{0.64}Si_{0.36}$ ($x = 0.00$, 0.01, 0.02, 0.03, 0.04, 0.05) MCMs were synthesized by solid-state chemical reaction, and the synthesis method is described in a previous paper [12]. To remove the so-called "virgin effect" a pre-cooling process in liquid nitrogen was chosen [26]. Zero-field differential scanning calorimetry (DSC) measurements were performed in a commercial TA-Q2000 DSC calorimeter (10 K/min), and in-field DSC characterization in a home-built Peltier cell-based instrument were carried out to derive the calorimetric ΔS_m and ΔT_{ad} [27,28]. XRD patterns were collected at a PANalytical X-pert Pro diffractometer with Cu K_α radiation and processed using Fullprof's implementation of the Rietveld refinement method [29]. The temperature-dependent magnetization (M-T) and field-dependent magnetization (M-H) curves were measured in a superconducting quantum interference device (SQUID, Quantum Design MPMS 5XL) magnetometer. Scanning electron microscopy (SEM) with energy-dispersive X-ray spectroscopy (EDX) was carried out on a JSM-IT100LA (JEOL) microscope to study the morphology and composition. To determine the W content within the matrix, as shown in Fig. S1 (Supporting Information), Electron Probe Micro Analysis (EPMA) measurement for $x = 0.05$ sample was conducted with a JEOL JXA 8900 R microprobe using an electron beam with energy of 10 keV and beam current of 200 nA employing Wavelength Dispersive Spectrometry (WDS). DFT calculations were performed via the Vienna *Ab* Initio simulation package (VASP) [30,31]. The projected augmented wave (PAW) method [32,33], was employed with the generalized gradient approximation of Perdew-Burke-Ernzerhof (PBE) as the exchange correlation functional [34]. The Methfessel-Paxton method [35] of the second order with a smearing width of 0.05 eV was used. In all calculations a $2 \times 2 \times 1$ supercell was relaxed on a k-grid of $5 \times 5 \times 11$ with an energy cut-off of 400 eV. A force convergence of 0.1 meV/Å and an energy convergence of 1 μeV were ensured. To determine the site preference of W, the formation energies for each possible doping site were calculated as $E_f = E_d + \mu_s - (E_p + \mu_W)$, where E_d and E_p are the energies of the doped and the pure compounds, while μ_W and μ_s are the chemical potentials of W and the substituted atoms.

3. Results and discussion

The specific heat as a function of temperature measured by zero-field DSC is shown in Fig. 1a. The observed endothermic and exothermic peaks indicate the presence of a FOMT. The significant decrease in peak height for high content W doping ($x \geq 0.04$) could be ascribed to the compositional variations. The inset shows that T_C continuously decreases upon W doping, while ΔT_{hys} remains almost constant at a relatively low value of about 5 K for $x \leq 0.04$ and then rapidly increases to 14.6 K for $x = 0.05$. As shown in Fig. 1b, the M-T curves in an applied field of 1 T present a sharp FOMT, that is conserved for low W contents ($x \leq 0.02$). For higher W contents ($x \geq 0.04$) the GMCE performance is expected to degrade as a result of the increase in ΔT_{hys}, the decrease in magnetization and the passivated FOMT. The inset clearly shows that the saturation magnetization (M_s) at 5 K decreased from 150.0 ($x = 0.00$) to 133.2 ($x = 0.05$) $Jkg^{-1}K^{-1}$ due to the substitution with non-magnetic W. The derived dM/dT indicates that for low W doping ($x \leq 0.02$) the T_C shift is 13.6 K/at% W and that ΔT_{hys} retains its very low level (below 4 K) upon W doping. It is worth to note that the obtained ΔT_{hys} from magnetic measurement is remarkably lower than that obtained from DSC as a result of the lower sweeping rate (2 K/min for M-T versus 10 K/min for DSC measurements) [36]. This very low value for ΔT_{hys} is

beneficial for the reversibility of the cooling/heating cycles [18,37,38]. The observation of a well-defined T_C shift with a constant ΔT_{hys} is rare for $(Mn,Fe)_2(P,Si)$ MCMs, compared with other substitutional/interstitial element doping elements in the form of: light elements (B, C, N, F, S) [11,12], 3d transition metal elements (V, Co, Ni, Cu, Zn) [13–15], 4d transition metal elements (Zr, Nb, Mo, Ru) [16–19] and other elements (Al, Ge, As) [1,20–22]. The difference between doping with W and doping with other elements could be ascribed to its unique outer electron configuration ($6s^24f^{14}5d^4$). The relatively high energy level of the 5d electrons may weaken its hybridization with metallic and non-metallic elements. As illustrated in Fig. 1d, to further evaluate the GMCE properties after W doping, the $|\Delta S_m|$ in different field changes is calculated from the Maxwell relation $\Delta S_m = \int_0^{\mu_0 H} (\frac{\partial M}{\partial T})_H dH$ for different W contents. Interestingly, the $|\Delta S_m|$ for $x \leq 0.02$ samples remains almost constant without degradation at values: for $x = 0.00$, 0.01 and 0.02 the values of $|\Delta S_m|$ are respectively 7.4(11.2), 7.7(11.6) and 6.5(11.4) $Jkg^{-1}K^{-1}$ for a magnetic field change of $\Delta \mu_0 H = 1(2)$ T. However, for $x \geq 0.04$ the FOMT character degrades and the $|\Delta S_m|$ value then gradually reduces for $x = 0.04$ and 0.05 to respectively 4.8(9.7) and 2.3(4.7) $Jkg^{-1}K^{-1}$ for $\Delta \mu_0 H = 1(2)$ T. The calorimetric ΔS_m and ΔT_{ad} have been derived for W doped samples by in-field DSC measurements. Note that the data from the Maxwell relation are shown for heating and cooling and the data from the in-field DSC only for heating. As illustrated in Fig. 1e, the $|\Delta S_m|$ from specific heat measurements is in good agreement with ones obtained from the Maxwell relation and the magnetization data for $\Delta \mu_0 H = 1$ T. Meanwhile, the determined ΔT_{ad}, which is another essential parameter for magnetic cooling/heating applications, also presents a conserved value of ΔT_{ad} with a shift in T_C for $x \leq 0.02$, in comparison with the undoped system. As shown in Fig. 1 f, for $x = 0.00$, 0.01 and 0.02 the ΔT_{ad} values respectively reach 2.5(3.9), 2.6(4.2) and 2.1(3.6) K for $\Delta \mu_0 H = 1(1.5)$ T. Thus, the ΔT_{ad} values for $x \leq 0.02$ are well conserved without remarkable degradation in low field changes. These ΔT_{ad} values are superior to the ones observed for magnetostructural NiMnIn(V) based Heusler alloys with $\Delta T_{ad} \approx 1.8$ K for $\Delta \mu_0 H = 1$ T [39] and the ones observed for all-d-metal NiCoMnTi(B) based Heusler alloys with $\Delta T_{ad} \approx 1.1$ K for $\Delta \mu_0 H$ = 1 T [38], which also show a good GMCE performance (measured at the same equipment). Note that all above ΔS_m and ΔT_{ad} values obtained from in-field DSC are collected at relative low field variations (less than 2 T), which suggests that these low W doped candidate materials could be applicable for the current Nd-Fe-B permanent magnets sources. Therefore, W alloying can not only tune the T_C shift without influencing ΔT_{hys}, but also conserves the well-constructed GMCE properties.

To better understand the relationship between structure changes and the performance, XRD patterns in the paramagnetic (PM) state (110 °C) have been refined to extract the crystallographic information. As presented in Fig. 2a the fit for the $x = 0.05$ sample indicates the presence of a cubic Fe_3W_3C based impurity phase (Fd-$3m$; space group 227). All refined XRD patterns can be found in Fig. S2 (Supporting Information). Early studies reported that Mn/Fe based carbides can even be produced in pure Mn-Fe-P-Si alloys, where the carbon source could originate from hydrocarbons during sealing the quartz tubes [40]. The ternary Fe-W-C phase diagram indicates that this Fe_3W_3C based compound can be formed above 1000 °C [41–43]. In Fig. 2b the obtained fraction of $(Mn,Fe)_3Si$ (impurity 1) (Fm-$3m$) [44] and Fe_3W_3C (impurity 2) based impurity phases shows that W doping significantly reduces $(Mn,Fe)_3Si$ from 6.2 ($x = 0.00$) to 0 ($x = 0.05$) wt%, while Fe_3W_3C starts to appear from $x = 0.03$ and keeps increasing with the W concentration. As indicated in Fig. 2c it is observed that the c/a ratio linearly increases for $x \leq 0.02$. The fluctuations for higher concentrations could be ascribed to a competition between impurity 1 and 2. It is worth to note that for this hexagonal ferromagnet the c/a ratio is closely associated to the
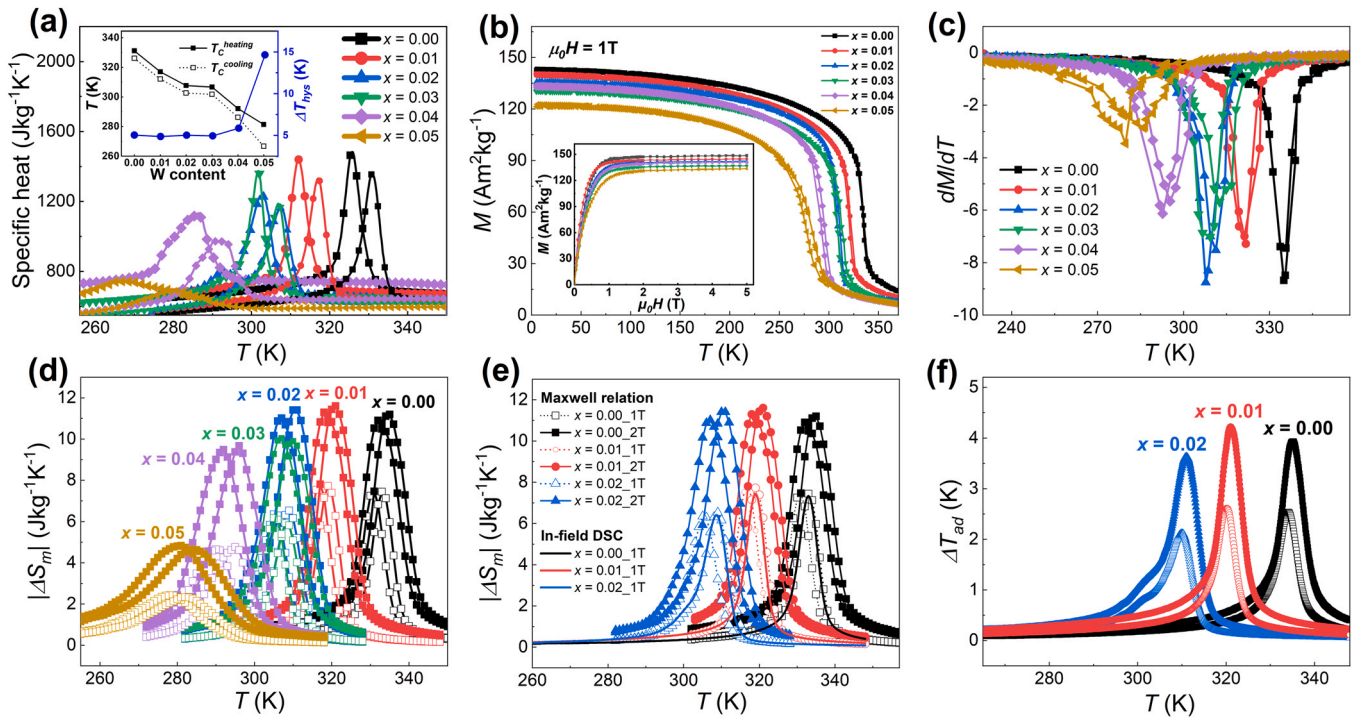
Fig. 1. (a) Specific heat derived from DSC experiments for $Mn_{0.6}Fe_{1.27-x}W_xP_{0.64}Si_{0.36}$ ($x = 0.00, 0.01, 0.02, 0.03, 0.04, 0.05$) materials upon heating and cooling. The inset is the changes of $T_C^{heating}$, $T_C^{cooling}$ and ΔT_{hys} as function of the W content. (b) Isofield M-T curves for different alloys at 1 T. The inset shows the corresponding M-H curves at 5 K. (c) Derived dM/dT curves for different W contents. (d) Calculated absolute ΔS_m values. (e) Comparison of absolute ΔS_m between the Maxwell calculation and calorimetric DSC measurements under low field changes. (f) Derived ΔT_{ad} values for low W contents. Note that solid and open symbols are for $\Delta\mu_0H = 1.0$ and 1.5 T, respectively.
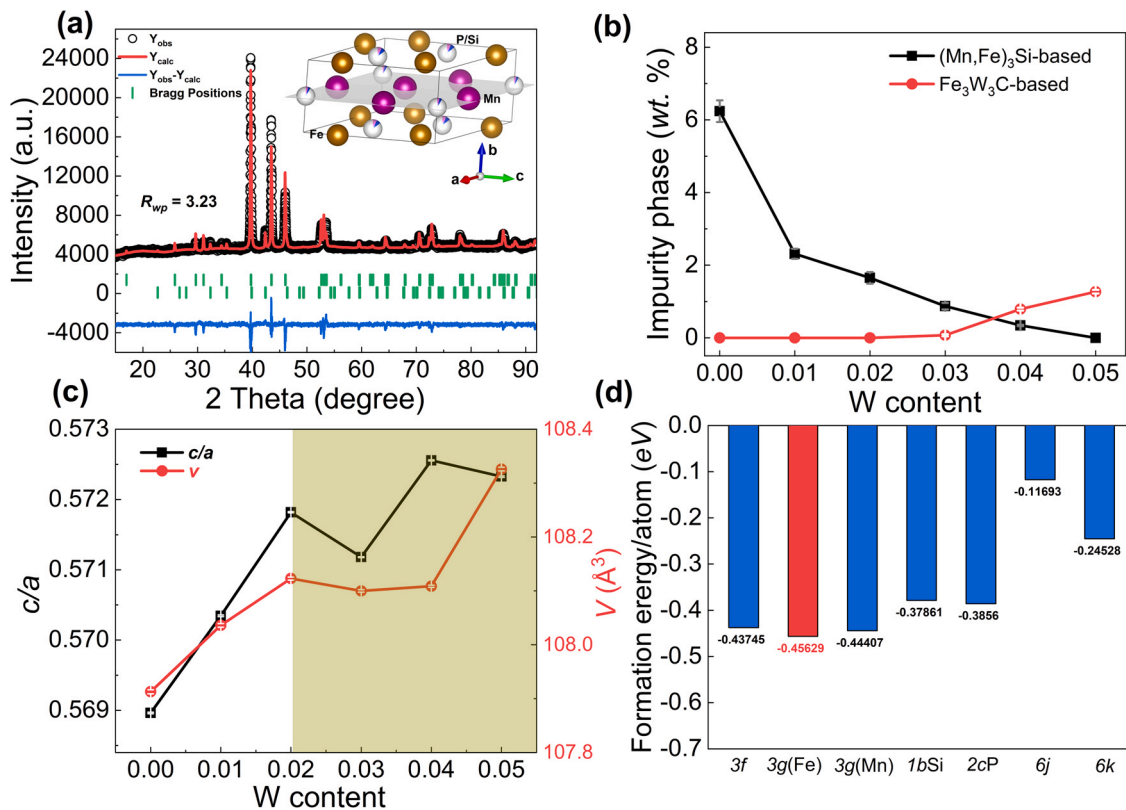

Fig. 2. (a) Refined XRD pattern (PM state) for the $Mn_{0.6}Fe_{1.22}W_{0.05}P_{0.64}Si_{0.36}$ sample. (b) Fraction of impurity phases for different W contents. (c) Derived c/a ratio and unit-cell volume V for different W contents. (d) Calculated E_f for different site-occupation models of W doped $(Mn,Fe)_2(P,Si)$ based materials.

Table 1

Summary of $T_C^{cooling}$, $T_C^{heating}$, ΔT_{hys}, lattice parameters a and c, c/a ratio, unit-cell volume V and impurity fractions for $Mn_{0.6}Fe_{1.27-x}W_xP_{0.64}Si_{0.36}$ (x = 0.00, 0.01, 0.02, 0.03, 0.04, 0.05) materials.

Sample	$T_C^{cooling}$ (K)	$T_C^{heating}$ (K)	ΔT_{hys} (K)	a (Å)	c (Å)	c/a	V (Å³)	Impurity 1 (wt%)	Impurity 2 (wt%)
x = 0.00	326.0	331.0	5.0	6.0277(1)	3.4296(5)	0.5690(1)	107.91(3)	6.2(3)	0
x = 0.01	312.1	317.0	4.9	6.0251(2)	3.4364(1)	0.5704(1)	108.04(1)	2.3(1)	0
x = 0.02	302.6	307.7	5.1	6.0216(1)	3.4432(5)	0.5718(2)	108.12(1)	1.7(2)	0
x = 0.03	301.8	306.7	4.9	6.0234(1)	3.4404(3)	0.5712(1)	108.10(1)	0.9(1)	0.07(3)
x = 0.04	286.2	292.0	5.8	6.0187(3)	3.4460(4)	0.5726(1)	108.10(1)	0.3(1)	0.79(4)
x = 0.05	266.7	281.3	14.6	6.0237(4)	3.4476(4)	0.5723(1)	108.34(1)	0	1.27(5)

strength of the magnetoelastic coupling [45–47]. The increase in c/a ratio (c axis expands and ab plane shrinks) indicates the weakened magnetic exchange interactions between the magnetic Mn/Fe atoms, which consequently lead to a reduction in T_C. The continuous increase in unit-cell volume indicates that the W atoms enter the matrix substitutionally, reflecting the bigger atomic covalent radius for W (r = 1.62 Å) in comparison with Fe (r = 1.32 Å) [48].

For highly ordered crystalline materials the precise atomic occupancy is indispensable for its own physical functionalities, for example the correlation between the ordering and GMCE [11,12,38,49,50]. Although X-ray diffraction cannot resolve the occupancy of Mn/Fe, the heavy element W can be clearly distinguished from Fe/Mn. It is found that W is located at the $3g$ site rather than the $3f$ site. In Fig. 2d the E_f obtained from DFT calculations for different site-occupation models of W doped $(Mn,Fe)_2(P,Si)$ materials is shown. The data clearly indicate that W prefers to occupy the substitutional $3g(Fe)$ site. The non-magnetic W substitution for Fe will dilute the magnetic moments, which is in good agreement with the reduced magnetization indicated in Fig. 1b and found in the DFT calculations. The $T_C^{cooling}$, $T_C^{heating}$, ΔT_{hys}, lattice parameters a and c, c/a ratio, unit-cell volume V and phase fractions (impurity 1 and 2) for the $Mn_{0.6}Fe_{1.27-x}W_xP_{0.64}Si_{0.36}$ (x = 0.00, 0.01, 0.02, 0.03, 0.04, 0.05) materials are summarized in Table 1.

As shown in Fig. 3, microstructural information has been obtained by applying SEM measurements. In Fig. 3a the microstructure for the x = 0.01 sample does not show W-based impurities but only cracks/holes/SiO_2 which are frequently generated for this quaternary alloy system [51]. Note that the trace amount of SiO_2 might be induced from the raw Si powder. In Fig. 3b it is clearly found that in the compound with x = 0.05 a dendritic-shaped W-based impurity phase is randomly distributed within the matrix with an average diameter of several μm (inset). This concomitant W-based impurity is detrimental to the mechanical properties. The EDX point scanning is applied to further establish the chemical composition of the different phases. The main phase is determined as $Mn_{0.73(5)}Fe_{1.38(6)}P_{0.56(2)}Si_{0.33(1)}W_x$ (W below the detection limit). To determine the content of doped W within the matrix, EPMA measurements were

applied. The chemical composition for the matrix phase of the x = 0.05 sample is found to be $Mn_{0.65(2)}Fe_{1.30(4)}P_{0.60(1)}Si_{0.43(7)}W_{0.021(1)}$. The lower concentration of the W dopant in main phase is expected to result from a limitation in the maximum W doping content for the higher W doped samples (x > 0.02). This is in agreement with the XRD results of the variation in unit-cell volume with the W doping content in Fig. 2c. Compared with the composition of the cubic W-based impurity ($(Fe_{2.4}W_3Mn_{0.5}P_{0.1}Si_{0.9})C_x$) extracted from SEM-EDX, the corresponding impurity composition for x = 0.05 sample is quantified from EPMA as $Fe_{2.7}W_3Mn_{0.5}P_{0.1}Si_{1.2}C_{1.2}$.

For this $(Mn,Fe)_2(P,Si)$ based MCM family with a magnetoelastic coupling the GMCE properties are controlled by the competition between the strong ferromagnetic exchange interaction and covalent bonding, which has been observed experimentally and theoretically (known as the so-called "mixed magnetism") [8,46,47]. For the present case, on the one hand, T_C is continuous reduced indicating the weakened exchange interactions among the magnetic atoms. The decreased intra-layer spacing for low content doping of W ($x \leq 0.02$) could potentially strengthen the covalent bonding between metallic – metallic and metallic – nonmetallic atoms due to an increase in orbital overlap between the outer electrons. This competition could be responsible for the relatively stable GMCE ($x \leq 0.02$), as presented in Fig. 1e–f. For $x \geq 0.03$ the GMCE performance is gradually degraded due to the appearance of the cubic Fe_3W_3C based impurity phase. Compared to the related Mo ($4d$ transition metal), W doping in $(Mn,Fe)_2(P,Si)$ MCMs behaves completely different. Mo substitution continuously reduces ΔT_{hys} and attenuates the GMCE performance [18], while W substitution ($x \leq 0.02$) conserves ΔT_{hys} at a very low level and maintains the GMCE. The difference could be ascribed to the difference in electron configuration between Mo ([Kr] $5s^14d^5$) and W ([Xe] $6s^24f^{14}5d^4$). Although they contain the same number of valence electrons (e_v = 6), Mo may more easily form an effective p-d hybridization with metalloids (P/Si) because its $4d$ energy level is markedly lower than the $5d$ energy level [52], which could lead to a weaker p–d hybridization for W. Meanwhile, the microstructural changes among different
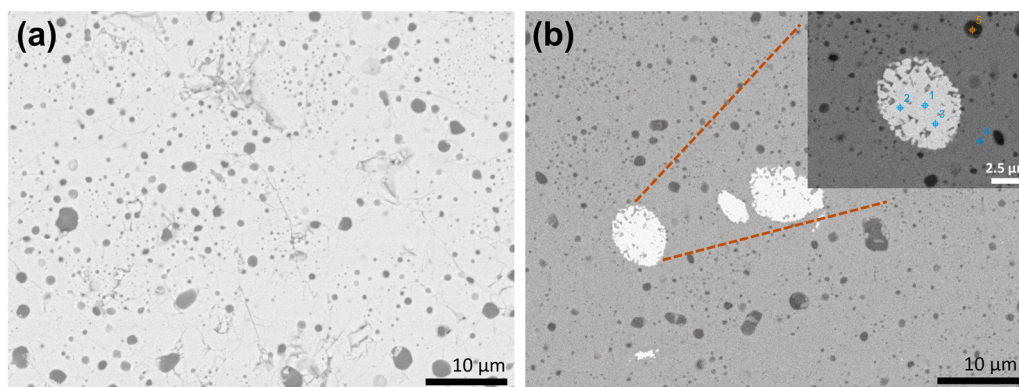

Fig. 3. (a) Back-scattered SEM image for the $Mn_{0.6}Fe_{1.26}W_{0.01}P_{0.64}Si_{0.36}$ alloy. (b) Back-scattered SEM image for the $Mn_{0.6}Fe_{1.22}W_{0.05}P_{0.64}Si_{0.36}$ alloy at the same magnification as (a). The inset shows the enlarged Fe_3W_3C based impurity phase.

competitive phases should also affect the influence of W substitution on the (Mn,Fe)$_2$(P,Si) based MCMs.

4. Conclusions

In summary, the effect of doping with the 5d element W has been studied for Fe-rich (Mn,Fe)$_2$(P,Si) based MCMs, and its influence on the thermodynamic properties, magnetic properties, crystalline structure and microstructure have been investigated. Compared with other metallic and non-metallic elements doping on this material system, which simultaneously move T_C and ΔT_{hys}, it is found that low content W substitution ($x \leq 0.02$) can only decrease T_C without influencing ΔT_{hys}. Though W doping does not further improve the MCE performance like other dopant, it is interesting to note that compared with the undoped material, low content W doping ($x \leq 0.02$) conserves the GMCE properties ($|\Delta S_m|$ and ΔT_{ad}), while for higher content W doping ($x \geq 0.03$) the corresponding properties are continuously weakened due to the formation of a Fe$_3$W$_3$C based impurity phase observed in XRD, SEM and EPMA. Therefore the 5d W doping (low content) maybe beneficial for designing the AMR bed materials. Combining XRD measurements and DFT calculations, the W atoms are found to substitutionally occupy the 3g(Fe) site. The competition between the magnetic exchange interactions and covalent bonding among different metallic and nonmetallic elements, is expected to be responsible for the observed behavior (tunable decrease in T_C, constant low value for ΔT_{hys} and the conserved MCE upon W doping).

CRediT authorship contribution statement

Fengqi Zhang: Conceptualization, Data curation, Formal analysis, Investigation, Writing – original draft, Writing – review & editing. **Sebastian Smits:** Data curation, Formal analysis, Investigation, Writing – review & editing. **Anika Kiecana:** Investigation, Writing – review & editing. **Ivan Batashev:** Investigation, Writing – review & editing. **Qi Shen**: Investigation, Writing – review & editing. **Niels van Dijk:** Conceptualization, Project administration, Supervision, Writing – review & editing. **Ekkes Brück:** Conceptualization, Project administration, Supervision, Writing – review & editing.

Data Availability

Data will be made available on request.

Declaration of Competing Interest

The authors declare that they have no known competing financial interests or personal relationships that could have appeared to influence the work reported in this paper.

Appendix A. Supporting information

Supplementary data associated with this article can be found in the online version at doi:10.1016/j.jallcom.2022.167802.

References

[1] D.T.C. Thanh, E. Brück, O. Tegus, J.C.P. Klaasse, K.H.J. Buschow, Influence of Si and Ge on the magnetic phase transition and magnetocaloric properties of MnFe(P, Si, Ge), J. Magn. Magn. Mater. 310 (2007) E1012–E1014.

[2] F. Guillou, G. Porcari, H. Yibole, N. van Dijk, E. Brück, Taming the first-order transition in giant magnetocaloric materials, Adv. Mater. 26 (2014) 2671–2675.

[3] O. Gutfleisch, M.A. Willard, E. Brück, C.H. Chen, S.G. Sankar, J.P. Liu, Magnetic materials and devices for the 21st century: stronger, lighter, and more energy efficient, Adv. Mater. 23 (2011) 821–842.

[4] T. Christiaanse, Characterization, Experimentation and Modeling of Mn-Fe-Si-P Magnetocaloric Materials., Ph.D. thesis, 2018.

[5] A. Kitanovski, J. Tušek, U. Tomc, U. Plaznik, M. Ožbolt, A. Poredoš, Magnetocaloric Energy Conversion, Springer, 2016.

[6] T. Christiaanse, E. Brück, Proof-of-concept static thermomagnetic generator experimental device, Met. Mater. Trans. E 1 (2014) 36–40.

[7] D. Dzekan, A. Waske, K. Nielsch, S. Fahler, Efficient and affordable thermomagnetic materials for harvesting low grade waste heat, Apl. Mater. 9 (2021) 011105.

[8] N.H. Dung, Z.Q. Ou, L. Caron, L. Zhang, D.T.C. Thanh, G.A. de Wijs, R.A. de Groot, K.H.J. Buschow, E. Brück, Mixed magnetism for refrigeration and energy conversion, Adv. Energy Mater. 1 (2011) 1215–1219.

[9] X. You, M. Maschek, N. van Dijk, E. Brück, Magnetic phase diagram of the MnxFe2-xP1-ySiy system, Entropy 24 (2022) 2.

[10] I. Batashev, G.A. de Wijs, N.H. van Dijk, E. Brück, Lithiation of the Fe2P-based magnetocaloric materials: a first-principles study, J. Magn. Magn. Mater. 537 (2021) 168179.

[11] X.F. Miao, N.V. Thang, L. Caron, H. Yibole, R.I. Smith, N.H. van Dijk, E. Brück, Tuning the magnetoelastic transition in (Mn,Fe)2(P,Si) by B, C, and N doping, Scr. Mater. 124 (2016) 129–132.

[12] F.Q. Zhang, I. Batashev, Q. Shen, Z.Y. Wu, R.I. Smith, G.A. de Wijs, N. van Dijk, E. Brück, Impact of F and S doping on (Mn,Fe)2(P,Si) giant magnetocaloric materials, Acta Mater. 234 (2022) 118057.

[13] J.W. Lai, B.W. Huang, X.F. Miao, N.V. Thang, X.M. You, M. Maschek, L. van Eijck, D.C. Zeng, N. van Dijk, E. Brück, Combined effect of annealing temperature and vanadium substitution for mangetocaloric Mn1.2-xVxFe0.75P0.5Si0.5 alloys, J. Alloy. Compd. 803 (2019) 671–677.

[14] Z.Q. Ou, N.H. Dung, L. Zhang, L. Caron, E. Torun, N.H. van Dijk, O. Tegus, E. Brück, Transition metal substitution in Fe2P-based MnFe0.95P0.50Si0.50 magnetocaloric compounds, J. Alloy. Compd. 730 (2018) 392–398.

[15] X.F. Miao, China Patent CN110343934B, 2019.

[16] J.T. Feng, F.J. Qian, D.N. Shi, H. Yang, Effect of Zr substitution on the crystal structure, magnetoelastic transition and magnetocaloric properties of (Mn,Fe)2(P,Si) alloys, Appl. Phys. 9 (2019) 358–364.

[17] S.Y. Hu, X.F. Miao, J. Liu, Z.Q. Ou, M.Q. Cong, O. Haschuluu, Y.Y. Gong, F.J. Qian, Y.R. You, Y.J. Zhang, F. Xu, E. Brück, Small hysteresis and giant magnetocaloric effect in Nb-substituted (Mn, Fe)2(P,Si) alloys, Intermetallics 114 (2019) 106602.

[18] X.F. Miao, Y. Gong, F.Q. Zhang, Y.R. You, L. Caron, F.J. Qian, W.H. Guo, Y.J. Zhang, Y.Y. Gong, F. Xu, N. van Dijk, E. Brück, Enhanced reversibility of the magnetoelastic transition in (Mn,Fe)2(P,Si) alloys via minimizing the transition-induced elastic strain energy, J. Mater. Sci. Technol. 103 (2022) 165–176.

[19] H. Wada, K. Nakamura, K. Katagiri, T. Ohnishi, K. Yamashita, A. Matsushita, Tuning the Curie temperature and thermal hysteresis of giant magnetocaloric (MnFe)2PX (X = Ge and Si) compounds by the Ru substitution, Jpn J. Appl. Phys. 53 (2014) 063001.

[20] D.M. Liu, H. Zhang, S.B. Wang, W.Q. Xiao, Z.L. Zhang, N. Tian, C.X. Liu, M. Yue, Q.Z. Huang, J.X. Zhang, J.W. Lynn, The effect of Al doping on the crystal structure and magnetocaloric behavior of Mn1.2Fe0.8P1-xGex compounds, J. Alloy. Compd. 633 (2015) 120–126.

[21] S. Kim, H. Shin, I. Chu, K. Lee, K.H. Lee, W. Lee, Tunable Curie temperature in Mn1.15Fe0.85P0.55Si0.45 via lattice engineering by Al addition, J. Alloy. Compd. 890 (2022) 161798.

[22] P. Wlodarczyk, L. Hawelek, M. Kowalczyk, M. Kaminska, P. Zackiewicz, M. Polak, M. Hreczka, A. Kolano-Burian, Impact of silicon doping on the magnetocaloric effect of MnFeP0.35As0.65 powder, Solid State Sci. 56 (2016) 23–28.

[23] F.Q. Zhang, C. Taake, B.W. Huang, X.M. You, H. Ojiyed, Q. Shen, I. Dugulan, L. Caron, N. van Dijk, E. Brück, Magnetocaloric effect in the (Mn,Fe)2(P,Si) system: from bulk to nano, Acta Mater. 224 (2022) 117532.

[24] L.F. Cohen, Contributions to hysteresis in magnetocaloric materials, Phys. Status Solidi B 255 (2018) 1700317.

[25] B. Huang, J.W. Lai, D.C. Zeng, Z.G. Zheng, B. Harrison, A. Oort, N.H. van Dijk, E. Brück, Development of an experimental rotary magnetic refrigerator prototype, Int. J. Refrig. 104 (2019) 42–50.

[26] X.F. Miao, L. Caron, Z. Gercsi, A. Daoud-Aladine, N.H. van Dijk, E. Brück, Thermal-history dependent magnetoelastic transition in (Mn,Fe)2(P,Si), Appl. Phys. Lett. 107 (2015) 042403.

[27] G. Porcari, F. Cugini, S. Fabbrici, C. Pernechele, F. Albertini, M. Buzzi, M. Mangia, M. Solzi, Convergence of direct and indirect methods in the magnetocaloric study of first order transformations: The case of Ni-Co-Mn-Ga Heusler alloys, Phys. Rev. B 86 (2012) 104432.

[28] G. Porcari, M. Buzzi, F. Cugini, R. Pellicelli, C. Pernechele, L. Caron, E. Brück, M. Solzi, Direct magnetocaloric characterization and simulation of thermomagnetic cycles, Rev. Sci. Instrum. 84 (2013) 073907.

[29] H.M. Rietveld, A profile refinement method for nuclear and magnetic structures, J. Appl. Crystallogr. 2 (1969) 65–71.

[30] G. Kresse, J. Hafner, Ab initio molecular dynamics for liquid metals, Phys. Rev. B 47 (1993) 558–561.

[31] G. Kresse, J. Furthmuller, Efficiency of ab-initio total energy calculations for metals and semiconductors using a plane-wave basis set, Comp. Mater. Sci. 6 (1996) 15–50.

[32] P.E. Blochl, Projector augmented-wave method, Phys. Rev. B 50 (1994) 17953–17979.

[33] G. Kresse, D. Joubert, From ultrasoft pseudopotentials to the projector augmented-wave method, Phys. Rev. B 59 (1999) 1758–1775.

[34] J.P. Perdew, K. Burke, M. Ernzerhof, Generalized gradient approximation made simple, Phys. Rev. Lett. 77 (1996) 3865–3868.

[35] M. Methfessel, A.T. Paxton, High-precision sampling for Brillouin-Zone integration in metals, Phys. Rev. B 40 (1989) 3616–3621.

[36] O. Gutfleisch, T. Gottschall, M. Fries, D. Benke, I. Radulov, K.P. Skokov, H. Wende, M. Gruner, M. Acet, P. Entel, M. Farle, Mastering hysteresis in magnetocaloric materials, Philos. Trans. R. Soc. A 374 (2016) 20150308.

[37] J. Liu, Y.Y. Gong, Y.R. You, X.M. You, B.W. Huang, X.F. Miao, G.Z. Xu, F. Xu, E. Brück, Giant reversible magnetocaloric effect in MnNiGe-based materials: minimizing thermal hysteresis via crystallographic compatibility modulation, Acta Mater. 174 (2019) 450–458.

[38] F.Q. Zhang, I. Batashev, N. van Dijk, E. Brück, Reduced hysteresis and enhanced giant magnetocaloric effect in B-Doped all-d-metal Ni-Co-Mn-Ti-based Heusler materials, Phys. Rev. Appl. 17 (2022) 054032.

[39] J. Liu, X.M. You, B.W. Huang, I. Batashev, M. Maschek, Y.Y. Gong, X.F. Miao, F. Xu, N. van Dijk, E. Brück, Reversible low-field magnetocaloric effect in Ni-Mn-In-based Heusler alloys, Phys. Rev. Mater. 3 (2019) 084409.

[40] T.D. Brown, D. Galvan, J. van Buskirk, A. Mott, P.J. Shamberger, Effect of carbide formation on phase equilibria and compositional modulation of transformation properties in (Mn,Fe)2(P,Si) alloys, J. Alloy. Compd. 830 (2020) 154532.

[41] C.B. Pollock, H.H. Stadelmaier, The eta carbides in the Fe−W−C and Co−W−C systems, Metall. Trans. 1 (1970) 767–770.

[42] M. Bergström, The Eta-carbides in the ternary system Fe-W-C at 1250 °C, Mater. Sci. Eng. 27 (1977) 257–269.

[43] P. Gustafson, A thermodynamic evaluation of the C−Fe−W system, Metall. Mater. Trans. A 18 (1987) 175–188.

[44] J.V. Leitao, X.M. You, L. Caron, E. Brück, Magnetostructural study of the (Mn,Fe)₃(P,Si) system, J. Alloy. Compd. 520 (2012) 52–58.

[45] E.K. Delczeg-Czirjak, Z. Gercsi, L. Bergqvist, O. Eriksson, L. Szunyogh, P. Nordblad, B. Johansson, L. Vitos, Magnetic exchange interactions in B-, Si-, and As-doped Fe2P from first-principles theory, Phys. Rev. B 85 (2012) 224435.

[46] M.F.J. Boeije, P. Roy, F. Guillou, H. Yibole, X.F. Miao, L. Caron, D. Banerjee, N.H. van Dijk, R.A. de Groot, E. Brück, Efficient room-temperature cooling with magnets, Chem. Mater. 28 (2016) 4901–4905.

[47] M. Maschek, X. You, M.F.J. Boeije, D. Chernyshov, N.H. van Dijk, E. Brück, Charge redistribution and the magnetoelastic transition across the first-order magnetic transition in (Mn,Fe)2(P,Si,B), Phys. Rev. B 98 (2018) 224413.

[48] B. Cordero, V. Gomez, A.E. Platero-Prats, M. Reves, J. Echeverria, E. Cremades, F. Barragan, S. Alvarez, Covalent radii revisited, Dalton Trans. 21 (2008) 2832–2838.

[49] X.F. Miao, L. Caron, P. Roy, N.H. Dung, L. Zhang, W.A. Kockelmann, R.A. de Groot, N.H. van Dijk, E. Brück, Tuning the phase transition in transition-metal-based magnetocaloric compounds, Phys. Rev. B 89 (2014) 174429.

[50] L.M. Moreno-Ramirez, C. Romero-Muniz, J.Y. Law, V. Franco, A. Conde, I.A. Radulov, F. Maccari, K.P. Skokov, O. Gutfleisch, The role of Ni in modifying the order of the phase transition of La(Fe,Ni,Si)13, Acta Mater. 160 (2018) 137–146.

[51] J.W. Lai, Z.G. Zheng, B.W. Huang, H.Y. Yu, Z.G. Qiu, Y.L. Mao, S. Zhang, F.M. Xiao, D.C. Zeng, K. Goubitz, E. Brück, Microstructure formation and magnetocaloric effect of the Fe2P-type phase in (Mn,Fe)2(P, Si, B) alloys, J. Alloy Compd. 735 (2018) 2567–2573.

[52] D.S. Kuiper, R.E. Douthwaite, A.R. Mayol, P.T. Wolczanski, E.B. Lobkovsky, T.R. Cundari, O.P. Lam, K. Meyer, Molybdenum and tungsten structural differences are dependent on nd(Z)2/(n+1)s mixing: comparisons of (silox)3MX/R (M = Mo, W; silox = (tBu3SiO)), Inorg. Chem. 47 (2008) 7139–7153.